Int. J. Heat Mass Transfer. Vol. 33, No. 2, pp. 301–317, 1990
Printed in Great Britain

0017–9310/90 $3.00 + 0.00

Theory of influence of a low-volatility, soluble impurity on spherically-symmetric combustion of fuel droplets

B. D. SHAW and F. A. WILLIAMS
Department of Applied Mechanics and Engineering Sciences, University of California, San Diego, La Jolla, CA 92093, U.S.A.

(*Received* 13 *December* 1988 *and in final form* 10 *May* 1989)

Abstract—Analyses are given for the evolution of liquid-phase mass fraction profiles and temperature during combustion of fuel droplets composed of binary miscible mixtures of low-volatility and high-volatility constituents, with small initial mass fractions of the low-volatility material, or slow introduction of low-volatility material into the liquid phase by absorption from the gas phase. The gas phase is assumed to remain quasisteady and the liquid temperature spatially uniform. The ratio of the liquid-phase diffusion coefficient to the initial burning-rate constant is treated as a small parameter. Asymptotic analyses in this parameter are developed, and the conservation equations are integrated numerically in obtaining descriptions of the combustion history. It is shown that at the surface of the droplet a boundary layer arises in which the mass fraction of the low-volatility component increases with time. The results are used to explain qualitatively some observed conditions of flame contraction and liquid disruption in droplet combustion.

1. INTRODUCTION

INFLUENCES of liquid-phase diffusion and volatility differences on the vaporization and combustion behavior of multicomponent droplets have been the subject of various theoretical, numerical, and experimental investigations because of their potential importance to the efficient utilization of fuel sprays as well as their fundamental interest. The earliest studies on multicomponent droplet combustion hypothesized that droplet combustion is a batch distillation process [1, 2]. However, more recent analyses have shown that liquid-phase diffusion can be important for situations in which significant volatility differences exist between fuel components, and where surface regression rates are fast compared with liquid-phase species diffusion rates. For example, Landis and Mills [3] report the results of numerical analyses concerning the spherically-symmetric evaporation (without combustion) of binary fuel droplets, demonstrating the effects of slow liquid-phase diffusion and volatility differentials. Results of similar numerical analyses are reported by Law [4]. Numerical analyses for binary fuel evaporation with and without combustion are also presented by Law and co-workers [5, 6], while experimental work in this area has also been active [5–10].

These analyses have been primarily concerned with the spherically-symmetric low-Reynolds-number evaporation and combustion of droplets. The results of these analyses have demonstrated, for binary fuel droplets with sufficiently different volatilities, that an initial transient period exists during which the more volatile component is preferentially evaporated, causing the droplet surface to regress. Surface regression, when sufficiently rapid, causes a 'boundary layer' of the less volatile component to develop near the droplet surface, increasing the mass fraction of the less volatile component at the droplet surface. For combustion (or evaporation in a hot environment) the droplet surface seeks to remain near the boiling temperature of the mixture at the surface. Hence, as the surface mass fraction of the less volatile component increases, the droplet surface temperature rises, increasing the evaporation rate of the less volatile component. This droplet heating has been shown to occur quite suddenly and rapidly after a period of d-square-law surface regression [5, 7] (the square of the droplet diameter decreasing linearly with time), causing reductions in flame diameters [5] as a result of reduced vaporization rates while heating occurs. Flame contraction is followed by flame growth, with another d-square-law period then possibly appearing, which may be terminated by disruption or extinction, or possibly by a batch distillation combustion regime [4]. The second d-square-law period is characterized by sufficiently vigorous evaporation of the less volatile component to prevent further buildup of its surface mass fraction. Since, in the situation described, chemical stratification within the droplet has occurred, the droplet interior may experience nucleation of the more volatile mixture if the droplet surface temperature is sufficiently high.

The analysis in this paper presents a parametric study concerned primarily with the early-time combustion behavior of fuel droplets containing a volatile component (termed in this paper 'fuel') and a miscible but low-volatility component (sometimes called an 'impurity'), where 'early time' here means prior to the

NOMENCLATURE

A	dimensionless parameter defined after equation (4)
B	transfer number
b_0	dimensionless parameter defined after equation (5)
c_p	gas-phase specific heat
c_ℓ	liquid-phase specific heat
D	liquid-phase species diffusivity
d	droplet diameter
E	dimensionless parameter defined after equation (19)
f	dimensionless gas-phase radial coordinate defined in equation (A4)
G	dimensionless measure of droplet burning rate defined by equation (19)
g, h, J	transformed liquid-phase mass fraction variables
h^0	enthalpy of formation
K	burning-rate constant
L	vaporization enthalpy
$\dot{m}$	droplet vaporization rate
P	pressure
q	chemical heat release
R	gas constant
r	radial coordinate
r_l	droplet radius
T	temperature
t	time
t_b	droplet burn time
$\hat{t}$	non-dimensional time defined in Section 3
V	droplet volume
W	molecular weight
X	mole fraction
x	dimensionless liquid-phase radial coordinate defined before equation (6)
Y, y	mass fraction
z	stretched liquid-phase radial coordinate defined before equation (7).

Greek symbols

α_i	coupling function variable defined in Appendix A
α_1, α_2	dimensionless reciprocal temperatures defined after equation (4)
β	dimensionless parameter defined after equation (5)
β'	scale factor between τ and τ' time scales
ε	inverse Peclet number, $8D_l/K$
$\tilde{\varepsilon}$	mass flux fraction
θ	non-dimensional temperature
λ	thermal conductivity
ν	chemical coefficient
ρ_l	liquid density
τ	non-dimensional transformed time defined before equation (5)
τ'	rescaled non-dimensional transformed time defined after equation (22)
φ	rescaled non-dimensional transformed time defined after equation (8)
Ω	coupling function defined in Appendix A
ω	ratio of fuel molecular weight to impurity molecular weight.

Subscripts

b	boiling
c	critical
F	fuel
H	impurity
I	gas-phase inert species
i, j	ith or jth species
O	oxidizer
P_i	ith product
SS	steady state
0	initial condition
+	condition of gas side of gas–liquid interface
−	condition on liquid side of gas–liquid interface
∞	condition at infinity.

above-mentioned flame contraction. The combustion behaviors of individual droplets will be studied; droplet interactions which may arise, for example, in dense sprays, are not considered. Approximate analyses will be presented to estimate the effects of liquid-phase species diffusion on the combustion behavior. The transient buildup of impurity profiles in droplets will be analyzed asymptotically and numerically under the assumptions that a quasisteady gas phase is present and that spherical symmetry exists in the liquid and gas phases.

Motivation for this work stems partly from the results of recent reduced-gravity combustion experiments in which multicomponent droplet behavior of the type described above was observed during the combustion of reasonably pure n-decane [11] or impure n-heptane [12] droplets. In these experiments, unsupported fuel droplets were observed to exhibit an initial period of approximately d-square-law combustion, followed by sudden flame contraction and then growth, and sometimes disruption. It has been suggested that this behavior can be attributed to the presence of one or more miscible, low-volatility impurities in the liquid phase, causing the type of multicomponent behavior discussed earlier. These impurities may have been initially present, or they

may have returned to the droplet from the gas phase as a result of fuel pyrolysis. Both types of impurity sources will be addressed here. Through parametric studies of the present type, ranges of conditions for the occurrence of the different types of observed behavior can be delineated with greater precision.

Three analyses concerning an initially present impurity will be presented. The first will be a numerical integration of the conservation equations for the case of an n-decane droplet undergoing combustion. This analysis will demonstrate that conditions may exist such that surface regression approximately follows the d-square-law until the surface mass fraction of impurity becomes of the order of unity, after which d-square-law surface regression is no longer approximately followed. The second analysis will be concerned with the evolution of impurity mass fraction profiles within a droplet with the assumption that surface regression follows d-square-law behavior. This analysis is needed for determining when the surface mass fraction of impurity approaches unity, signalling that d-square-law surface regression is no longer maintained (e.g. when flame contraction through droplet heating begins). The third analysis will consider non-d-square-law droplet combustion related to droplet heating. All of these analyses will assume that impurity vaporization is negligible. Estimates regarding conditions under which this assumption is valid will be presented.

Analyses addressing the possibility of low-volatility impurities returning from the gas phase to the liquid phase will be presented for the purpose of identifying conditions under which combustion behavior may be significantly influenced by the returning impurities. These analyses parallel those described above, but with altered boundary conditions.

In all analyses, liquid-phase heat conduction is assumed to be sufficiently rapid that temperature profiles in the liquid phase are spatially uniform but time varying. This permits a significant simplification in the equations describing the droplet combustion. A partial justification for this assumption is that previous investigators have shown that transient droplet heating effects on vaporization rates can be adequately modeled in this manner for many single-component fuels [13]. Since vaporizing multicomponent droplets have approximately the same liquid-phase thermal diffusivities as single-component fuels, it may be conjectured that this approximation will remain equally useful. For accurate analysis of disruption events, however, thermal gradients in the liquid phase may need to be considered. The present work does not specifically address disruption but focuses instead on vaporization rates of droplets.

2. FORMULATION

Consider a droplet with a miscible impurity of very low volatility that is undergoing spherically-symmetric combustion. The temperature at the droplet surface will tend to approach closely the equilibrium boiling temperature of the mixture at the surface. Hence, for the situation in which impurity is present at the surface in small amounts, the surface temperature will be near that of the boiling point of the high-volatility fuel constituent (under steady conditions). As the fuel vaporizes, the droplet surface regresses, causing the mass fraction of impurity to increase if impurity vaporization is sufficiently weak. Conditions for neglecting impurity vaporization will be discussed later. Increases of impurity mass fraction at the droplet surface lead to increases in the droplet surface temperature.

With the assumption that thermal gradients within the droplet are negligible, formally derivable by taking the limit of infinite ratio of liquid to gas thermal conductivity, the energy equation for the liquid phase is

$$\frac{\rho_l c_c r_l}{3}\frac{\mathrm{d}T}{\mathrm{d}t} = \left(\lambda\frac{\partial T}{\partial r}\right)_+ + \rho_l L\frac{\mathrm{d}r_l}{\mathrm{d}t} \qquad (1)$$

subject to the initial condition $T(0) = T_0$, where c_c is the specific heat of the liquid, r_l the droplet radius, ρ_l the liquid density, T the temperature, L the enthalpy of vaporization per unit mass, t the time, and λ the gas-phase thermal conductivity. When multiple species are entering or leaving the liquid phase, L can be assumed to be given by $L = \Sigma_i \bar{\varepsilon}_i L_i$ where $\bar{\varepsilon}_i$ is the mass-flux fraction of the ith species, and L_i the vaporization enthalpy of the ith species. Throughout this paper c_c and ρ_l are assumed constant. The subscript + denotes that the quantity in question is evaluated on the gas side of the liquid–gas interface.

For a quasisteady gas phase, it is shown in Appendix A that the temperature gradient on the gas side of the liquid–gas interface can be approximately evaluated in terms of physicochemical properties and the dimensionless burning rate f (see equation (A7)) yielding

$$\frac{\rho_l c_c c_p}{3\lambda L} r_l^2 \frac{\mathrm{d}T}{\mathrm{d}t} = f\left[\frac{B}{\mathrm{e}^f - 1} - 1\right], \quad T(0) = T_0 \qquad (2)$$

where c_p is the gas-phase specific heat, and $B = [c_p(T_\infty - T) + qY_{O,\infty}/(\nu_O W_O)]/L$ is a transfer number. When f is constant, droplet surface regression follows the d-square-law. Here, T_∞ and $Y_{O,\infty}$ are the ambient temperature and oxidizer mass fractions, respectively, and $q/(\nu_O W_O)$ the chemical heat released per unit mass of oxidizer consumed in the gas phase. The derivation of equation (2) from equation (A4) evaluated at $r = r_l$ involves the further approximation that λ/c_p for the gas is constant, an approximation that will be used for simplicity throughout the present analysis.

The function f in equation (2) is related to Y_+, the gas-phase mass fraction of fuel at the liquid–gas interface, by equation (A10), which can be written as

$$\mathrm{e}^f = (1 - \bar{\varepsilon} + \nu)/(1 - \bar{\varepsilon} - Y_+) \qquad (3)$$

where $v \equiv Y_{O,\infty} \nu_F W_F/(\nu_O W_O)$, and $\bar{\varepsilon}$ is the mass-flux fraction of impurity from the droplet surface. For convenience, ideal-solution behavior and applicability of the Clausius–Clapeyron equation with constant vaporization enthalpy [14] will be assumed adequate in describing the phase-change behavior. Equations (A12)–(A15) can then be combined with equation (3) to yield

$$1+A/[(1-\bar{\varepsilon})(e^f-1)-v] = [1+\omega y_-/(1-y_-)] \times \exp[\alpha_1^2/(\theta+\alpha_1)-\alpha_2] \quad (4)$$

where $\omega = W_F/W_H$, $\alpha_1 = L_F/(R_F T_0)$, $\alpha_2 = L_F/(R_F T_{bF})$, $A = [(W_F Y_{O,\infty})/(\nu_O W_O)] \Sigma_j \nu_{P_j} + (W_F/W_I) \times (1-Y_{O,\infty})$, and $\theta = L_F(T-T_0)/R_F T_0^2$. Here L_F is the fuel vaporization enthalpy, R_F the gas constant for the fuel, W_F the fuel molecular weight, W_H the impurity molecular weight, W_I the gas-phase inert molecular weight, y_- the mass fraction of impurity at the droplet surface in the liquid phase, and T_{bF} the boiling temperature for pure fuel.

In terms of the dimensionless temperature θ and the dimensionless time $\tau = \ln(r_{l0}/r_l)$ (where r_{l0} is the initial droplet radius), equation (2) becomes

$$\beta \frac{d\theta}{d\tau} = \frac{B}{e^f-1} - 1, \quad \theta(0) = 0 \quad (5)$$

where the constant $\beta = c_c R_F T_0^2/(3LL_F)$, and L has been assumed constant. When impurity vaporization is negligible, $L = L_F$; when impurity is returning to the surface its heat of vaporization provides a negative contribution to L. In equation (5) $B = B_0 - b_0\theta$, where $B_0 \equiv [c_p(T_\infty - T_0) + qY_{O,\infty}/(\nu_O W_O)]/L$ and $b_0 \equiv c_p R_F T_0^2/(LL_F)$ are constants.

The energetic aspects of the problem are defined nondimensionally by equations (4) and (5). There are eight parameters appearing in these equations, namely, β, B_0, b_0, A, v, ω, α_1, and α_2. Equation (5) is a non-linear first-order ordinary differential equation for θ as a function of τ, in which the variable f appears. Equation (4) relates f to θ, $\bar{\varepsilon}$ and y_-. The equation for conservation of impurity in the liquid phase must be considered to find y_-.

With spherical symmetry, liquid-phase conservation of impurity can be assumed to be described by the partial differential equation

$$\frac{\partial y}{\partial t} = \frac{D}{r^2}\frac{\partial}{\partial r}\left(r^2 \frac{\partial y}{\partial r}\right)$$

subject to the boundary conditions

$$\left(D\frac{\partial y}{\partial r} + y\frac{dr_l}{dt}\right)_{r=r_l} = \bar{\varepsilon}\frac{dr_l}{dt}, \quad \left(\frac{\partial y}{\partial r}\right)_{r=0} = 0$$

and the initial condition $y(r,0) = y_0$. Here, D is the (constant) liquid-phase species diffusion coefficient of the impurity, y the impurity mass fraction, and r the radial coordinate. Use has been made of the previously stated assumption that droplet density changes are negligible. Impurity vaporization is negligible when $\bar{\varepsilon}$ is sufficiently small. The initial analysis assumes that $\bar{\varepsilon}$ is small and can be neglected, although it will be taken into account as an additional constant parameter when return of impurity from the gas is considered.

If the transformations $x = r/r_l$ and $d\tau = d\ln(r_{l0}/r_l)$ are used, then with $\varepsilon = -D/[r_l(dr_l/dt)]$ the liquid-phase problem becomes

$$\frac{\partial y}{\partial \tau} = \frac{\varepsilon}{x^2}\frac{\partial}{\partial x}\left[x^2\frac{\partial y}{\partial x}\right] - x\frac{\partial y}{\partial x}$$

$$\left(\varepsilon\frac{\partial y}{\partial x} - y\right)_{x=1} = -\bar{\varepsilon}, \quad \left(\frac{\partial y}{\partial x}\right)_{x=0} = 0. \quad y(x,0) = y_0. \quad (6)$$

The definition $K \equiv -8r_l(dr_l/dt)$ of the burning-rate constant can be used, yielding the d-square-law given by equation (A19) when K is constant. The physical time t and non-dimensional time τ are related by $t = (c_p r_{l0}^2 \rho_l/\lambda)\int_0^\tau (e^{-2\tau}/f)\,d\tau$. The term ε can be recast as $\varepsilon = D\rho_l c_p/(\lambda f) = \varepsilon_0 f_0/f$ where $\varepsilon_0 = 8D/K_0$ and $f_0 = \rho_l c_p[r_l(dr_l/dt)]_0/\lambda_+$. The subscript 0 used here indicates that the quantities in question are evaluated at $\tau = 0$.

Equations (4)–(6) will be assumed to describe the behavior of an isolated fuel droplet undergoing spherically-symmetric combustion with a low-volatility impurity present in the liquid phase. Equation (6) will serve to determine y_- but has been seen to introduce four new parameters, ε_0, f_0, $\bar{\varepsilon}$, and y_0. Therefore, there are a total of 12 parameters in the complete problem, giving a wide range of possible behaviors. The system of equations will be studied only for particular orderings of the parameters, selected for correspondence to the most realistic physical situations.

3. NUMERICAL ANALYSIS

Equations (4)–(6) with $\bar{\varepsilon} = 0$ were integrated numerically for an n-decane droplet undergoing combustion in an atmosphere containing mass fractions of 50% O_2 and N_2, respectively. Combustion products were selected to be H_2O and CO_2. The integrations were performed using the values $\omega = 0.2$, $A = 5.5418$, $v = 0.1431$, $\alpha_2 = 10.57$, $b_0 = 0.61$, $D = 5\times10^{-9}$ m^2 s^{-1}, $\rho_l = 603.3$ kg m^{-3}, $c_c = 2141$ J kg^{-1} K^{-1}, $c_p = 4200$ J kg^{-1} K^{-1}, $T_\infty = 300$ K, $\lambda = 0.1627$ J m^{-1} s^{-1} K^{-1}, and $q/(\nu_O W_O) = 12.61$ MJ kg^{-1}, corresponding to $\beta = 0.104$ and $B_0 = 20.7$. The magnitude for D was selected to provide a reasonable intermediate value for the liquid-phase diffusion coefficient. The parameter y_0 was either 0.02 or 0.1. For $y_0 = 0.02$, $\alpha_1 = 10.80$, $f_0 = 3.08$, and $\varepsilon_0 = 0.025$, while for $y_0 = 0.1$, $\alpha_1 = 10.79$, $f_0 = 3.07$, and $\varepsilon_0 = 0.026$, corresponding to initial quasisteady combustion. The variable T_0 was selected such that equations (4) and (5) were satisfied for the right-hand side of equation (5) vanishing. This temperature corresponds to the temperature a droplet would attain if

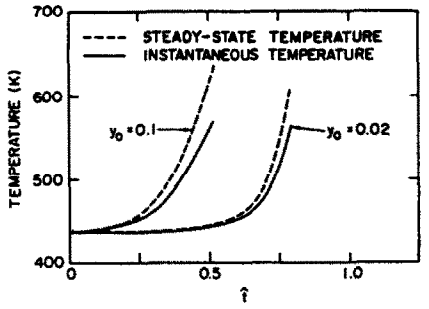

FIG. 1. Variations of the temperature T with time for an n-decane droplet undergoing combustion with an initial impurity mass fraction of $y_0 = 0.1$ or 0.02.

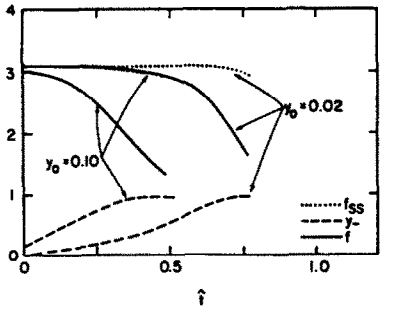

FIG. 2. Variations of the impurity surface mass fraction y_- and the non-dimensional burning rate f with time for an n-decane droplet undergoing combustion with an initial impurity mass fraction of $y_0 = 0.1$ or 0.02.

surface impurity buildup did not occur and surface regression followed the d-square-law. Evolution of the impurity profiles was determined by evaluating equation (6) with a Crank–Nicolson scheme [15], while equation (5) was evaluated using the Euler method [15]. The equations were found to be numerically stiff so that a large number of grid points and small time steps had to be used. The grid spacing in the spatial coordinate was $\Delta x = 1/900$ for the results presented here. The time steps for the results presented were $\Delta\tau = 0.0002$ for $y_0 = 0.02$, and $\Delta\tau = 0.0001$ for $y_0 = 0.1$. These time steps were reduced by a factor of 20 when the impurity surface mass fraction approached unity. This reduction was necessary because equation (5) became progressively stiffer as y_- approached unity. Further reductions in the time steps before the impurity surface mass fraction approached unity, and further increases in the number of grid points used did not change the results significantly.

Shown in Fig. 1 are results for the instantaneous physical droplet temperature and the 'steady-state' physical droplet temperature plotted as functions of the non-dimensional physical time $\hat{t} = 2t\lambda[\ln(1+B_0)]/(c_p r_{i0}^2 \rho_l)$ for $y_0 = 0.02$ and 0.1. The time $\hat{t}$ would reach unity when the droplet disappears if the burning-rate constant were invariant. Steady-state droplet temperature is defined in Fig. 1 as the temperature the droplet would attain for equations (4) and (5) being satisfied with the right-hand side of equation (5) vanishing. The solid lines are the instantaneous temperature and the broken lines are the steady-state temperature. Figure 1 indicates that the instantaneous droplet temperature lags progressively further behind the steady-state temperature as combustion progresses. The temperature lag appears as a result of increases in y_-. As y_- increases, the droplet requires heating. Because the droplet has a finite mass and heat capacity, it cannot heat instantaneously, so the instantaneous temperature lags behind the steady-state temperature. This lag occurs earlier and is of greater magnitude for $y_0 = 0.1$ than for $y_0 = 0.02$. This is a result of the lessened droplet heating-rate requirements for $y_0 = 0.02$. Shown in Fig. 2 are results for f and y_- as functions of t for $y_0 = 0.1$ and 0.02. Also plotted are results for f_{ss}, which is the value that f would achieve for the given y_- if the droplet temperature followed the steady-state profile shown in Fig. 1. The f values are the solid lines, the y-values are the broken lines, and the f_{ss} values the dotted lines. Evident in Fig. 2 is the trend that f is approximately constant until the surface mass fraction of impurity approaches unity, after which f decreases significantly. The variable f_{ss} changes much more slowly than f as $y_- \to 1$, indicating that droplet heating is important as $y_- \to 1$ (i.e. the droplet cannot heat rapidly enough to maintain vaporization levels as given by f_{ss}). Comparison of Figs. 1 and 2 illustrates that large changes in f and significant temperature lags occur as $y_- \to 1$ closely. Decreases in f are more gradual for $y_0 = 0.1$ than for $y_0 = 0.02$, and the period of approximately constant f is greater for $y_0 = 0.02$ than for $y_0 = 0.1$. These phenomena will be discussed in more detail later in this paper.

Computer runs were also made for different values of oxygen concentration in the atmosphere, for different values of y_0, and also for n-heptane. The results from these runs, not presented here, generally followed the trends presented earlier in that for sufficiently small values of y_0 an initial period existed during which f was approximately constant and the instantaneous droplet temperature closely followed the steady-state droplet temperature. As combustion proceeded and the impurity surface mass fraction approached unity, f decreased significantly and substantial temperature lags appeared. The decrease in f was found to occur more suddenly as y_0 and ω were decreased. Increasing y_0 tended to cause decreases in f to occur more gradually.

4. ANALYSIS OF EARLY d-SQUARE-LAW COMBUSTION BEHAVIOR

The numerical results presented earlier suggest that for sufficiently small y_0, an early period of combustion exists during which f is approximately constant until $y_- \to 1$. For constant f, equation (6) with $\varepsilon = \varepsilon_0$ and

$\tilde{\varepsilon} = 0$ can be solved to estimate the buildup of impurity at the droplet surface.

Under typical droplet combustion situations $K_0 \sim 10^{-6}$ m^2 s^{-1}, while $D \sim 10^{-9}$ m^2 s^{-1}, yielding $\varepsilon = \varepsilon_0 = 8D/K_0 \sim 10^{-2}$. Hence ε can be considered a small parameter, and asymptotic analyses can be performed for the limit $\varepsilon \to 0$. Having $\varepsilon \ll 1$ indicates that liquid diffusion is much slower than surface regression, suggesting that a 'boundary layer' of impurity will exist at the droplet surface. This has been emphasized recently by Makino and Law [16].

Since a boundary layer of impurity is expected near the droplet surface, the substitution $x = 1 - \delta z$ is appropriate. Here z is the 'stretched' variable and δ is a small parameter to be determined. With the transformation $h = y/y_0 - 1$, the problem in the boundary layer becomes

$$\frac{\partial h}{\partial \tau} = \frac{1}{\delta}\frac{\partial^2 h}{\partial z^2} - \frac{2\varepsilon}{\delta}\frac{1}{1-\delta z}\frac{\partial h}{\partial z} + (1-\delta z)\frac{1}{\delta}\frac{\partial h}{\partial z}$$

$$\left(\frac{\varepsilon}{\delta}\frac{\partial h}{\partial z} + h\right)_{z=0} = -1, \quad h(z,0) = 0, \quad h(z \to \infty) = 0. \tag{7}$$

A distinguished limit is found by setting $\delta = \varepsilon$ (see Appendix B for details), yielding the leading-order problem

$$\frac{\partial h_0}{\partial \varphi} = \frac{\partial^2 h_0}{\partial z^2} + \frac{\partial h_0}{\partial z}, \quad \left(\frac{\partial h_0}{\partial z} + h_0\right)_{z=0} = -1$$

$$h_0(z,0) = 0, \quad h_0(z \to \infty) = 0 \tag{8}$$

where $\varphi = \tau/\varepsilon$ is a 'stretched' time and h_0 the leading-order term of the inner expansion $h = h_0 + \varepsilon h_1 + \ldots$ The condition $h_0(z \to \infty) = 0$ is found by matching to the outer solution, where it is found that the solution outside the boundary layer must be $h = 0$ (see Appendix B). For small diffusion rates this is physically satisfactory. The solution to this leading-order boundary-layer analysis is

$$(y/y_0) = h_0 + 1 = (e^{-z}/2)(\varphi - z + 1)$$
$$\times [1 + \operatorname{erf}(\sqrt{(\varphi/4)} - z/\sqrt{(4\varphi)}] - 1/2 \operatorname{erfc}[\sqrt{(\varphi/4)}$$
$$+ z\sqrt{(4\varphi)}] + \sqrt{(\varphi/\pi)} \exp[-(z^2/\varphi + 2z + \varphi)/4] + 1 \tag{9}$$

as shown in Appendix B. At the droplet surface ($z = 0$) equation (9) reduces to

$$(y/y_0)_- = (\varphi/2)[1 + \operatorname{erf}\sqrt{(\varphi/4)}] + \operatorname{erf}\sqrt{(\varphi/4)}$$
$$+ \sqrt{(\varphi/\pi)}\, e^{-\varphi/4} + 1. \tag{10}$$

The physical situation described by the leading-order boundary-layer problem (equation (8)) is that of a planar boundary regressing with constant velocity into a semi-infinite medium. Because a droplet reduces its surface area as it vaporizes, it is expected that this solution will be approximately valid until the droplet surface area changes appreciably, reducing the effective volume available to the impurity, thereby causing a faster buildup of impurity at the surface than predicted by equation (10). Equation (10) can be expected to provide increasingly accurate estimates for the buildup of impurity at the droplet surface to a mass fraction of the order of unity for increasing values of y_0. For $\tau \ll \varepsilon$, equation (10) shows that $(y/y_0)_- \approx 1 + \sqrt{(\tau/(\varepsilon\pi))}$, while for $\varepsilon \ll \tau$, equations (9) and (10) are approximately described by

$$(y/y_0) \approx \tau e^{-z}/\varepsilon + 1 \tag{11}$$

and

$$(y/y_0)_- \approx \tau/\varepsilon + 1. \tag{12}$$

Equation (11) shows the boundary-layer structure, and equation (12) demonstrates a linear buildup of surface mass fraction of the heavy constituent with τ. In Appendix B it is demonstrated that the next term in the inner expansion for h goes approximately as $h_1 \approx 3\varphi^2/2$ for $\varphi \to \infty$, indicating that the leading-order solution is valid for $\tau \ll 1$. Since $\tau = -(1/2) \times \ln(1 - t/t_b)$ (where $t/t_b = tK_0/(4r_{s0}^2)$ is the fractional burn-time elapsed) the leading-order analysis is restricted to $t/t_b \ll 1$ (the early portions of the droplet lifetime). This makes sense physically, because for $t/t_b \ll 1$, only small changes in droplet surface area will have occurred. In physical coordinates, equation (12) predicts that the impurity mass fraction at the droplet surface increases approximately as

$$y_- \approx y_0\{1 - [1/(2\varepsilon)] \ln(1 - t/t_b)\} \tag{13}$$

valid for the time range $\varepsilon \ll t/t_b \ll 1$, within which range $\ln(1 - t/t_b) \approx -t/t_b$.

With the substitution $J = y/y_0$, equation (6) with $\tilde{\varepsilon} = 0$ was integrated numerically using an IMSL PDE solver (DMOLCH) [17]. The IMSL routine required as input initial conditions which satisfied the boundary conditions of the PDE. Inspection of equation (6) shows that at $\tau = 0$, the initial conditions do not satisfy the boundary conditions. As a result, the IMSL routine was 'started' at a time $\tau > 0$ by using as input initial conditions generated by using the leading-order asymptotic solution (equation (9)), valid as $\tau \to 0$, with the initial condition adjusted slightly near $x = 0$ to satisfy the zero gradient. The 'start' time used was $\tau = 0.001$. As a check of the accuracy of these computations, equation (6) was also integrated using a Crank–Nicolson routine [15]. Results between the IMSL and Crank–Nicolson routines were found to agree very closely.

Shown in Fig. 3 are numerically-generated and asymptotic leading-order results for the surface mass fraction ratio $(y/y_0)_-$ as a function of the physical burn-time ratio t/t_b and τ for $\varepsilon = 0.02$ and 0.05. Good agreement can be observed between the numerical and asymptotic analyses for $t/t_b \to 0$. For $t/t_b \gtrsim 0.1$, the numerical results exhibit significantly more curvature than the asymptotic results. The asymptotic results for $(y/y_0)_-$ in Fig. 3 lag progressively further behind the numerical results with increasing τ. As discussed

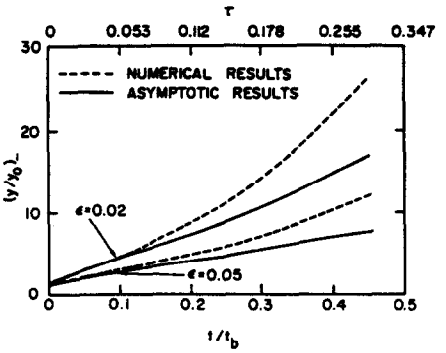

FIG. 3. Comparison of numerical and early-time asymptotic solutions of equation (6) for the surface impurity mass fraction ratio $(y/y_0)_-$ as a function of time.

previously, this lag arises because the asymptotic results are for planar motion in a semi-infinite domain, where the surface area is constant, while the numerical results account for droplet sphericity and changes in droplet surface area and volume.

Figure 4 gives plots of the numerically-computed and asymptotic impurity mass-fraction profiles as a function of the normalized droplet radius for $\varepsilon = 0.02$ and 0.05, respectively. For each plot, $t/t_0 = 0.1813$ ($\tau = 0.1$). The numerical and asymptotic profiles are quite similar, except that a higher value of the surface mass fraction ratio is predicted by the numerical analysis for this particular time, as shown in Fig. 3 and explained above.

Figure 3 indicates that equation (9) can be expected to be valid until $t/t_b \approx 0.1$. Equation (13) can be solved for y_0 to estimate the minimum value of y_0 allowed to produce $y_- = O(1)$ at a burn-time ratio of $t/t_b \cong 0.1$. For $y_- = 1$, $\varepsilon = 0.02$, and $t/t_b = 0.1$, equation (13) requires that $y_0 \gtrsim 0.28$ for equations (9) and (13) to be useful for estimating the time required for the impurity mass fraction at the surface to approach unity. For $\varepsilon = 0.05$, $t/t_b = 0.1$ and $y_- = 1$, equation (13) yields $y_0 \gtrsim 0.49$, while for $\varepsilon = 0.01$ equation (13) yields $y_0 \gtrsim 0.16$. Since these values of y_0 are larger than is normally encountered, there is motivation for seeking improved approximations that take into account the volume change of the droplet.

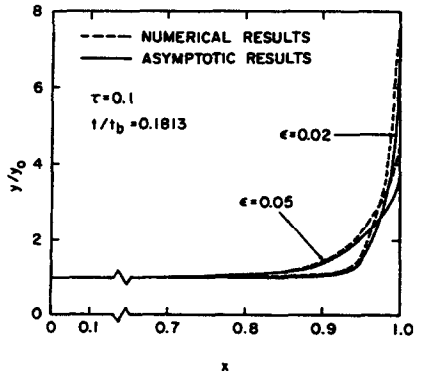

FIG. 4. Comparison of numerical and early-time asymptotic solutions of equation (6) for the spatial profile of the mass fraction impurity ratio (y/y_0) at the time $t/t_b = 0.1813$.

5. LATER *d*-SQUARE-LAW COMBUSTION BEHAVIOR

To extend the region of validity of the previous asymptotic analysis to larger values of time, more terms in the formal asymptotic expansion can be computed. This method, however, is quite involved (Appendix B). An alternative approach is to transform the dependent coordinate according to $y = y_0(g+1)$ yielding the problem

$$\frac{\partial g}{\partial \tau} = \varepsilon \frac{\partial^2 g}{\partial x^2} + \left[\frac{2\varepsilon}{x} - x\right]\frac{\partial g}{\partial x}$$

$$\left[\varepsilon \frac{\partial g}{\partial x} - g\right]_{x=1} = 1, \quad \left(\frac{\partial g}{\partial x}\right)_{x=0} = 0, \quad g(x,0) = 0. \tag{14}$$

To analyze equation (14), it is advantageous to take a Laplace transform in the time coordinate, yielding an ordinary differential equation for the transformed dependent variable in terms of the transform variable s and the spatial coordinate x (see Appendix C for details of this analysis). An exact solution to the ordinary differential equation can be found, but the inverse transformation of this solution was not evaluated because of the complexity of the solution. An approximate solution can be found, however, by WKB analysis [18], which can be easily transformed back to the original time variable. From the WKB analysis, the physical-optics approximation for the mass fraction ratio for $\tau \gg \varepsilon$ is

$$(y/y_0) \approx 1 + [1/(3\varepsilon)](e^{3\tau} - 1)\exp[(x^2-1)/(2\varepsilon)]. \tag{15}$$

In physical time this relation becomes

$$(y/y_0) \approx 1 + [1/(3\varepsilon)][(1-t/t_b)^{-3/2} - 1] \times \exp[(x^2-1)/(2\varepsilon)]. \tag{16}$$

Since for *d*-square-law behavior $(V/V_0) = (1-t/t_b)^{3/2}$, equation (16) can be rewritten as

$$(y/y_0) \approx 1 + [1/(3\varepsilon)](V_0/V - 1)\exp[(x^2-1)/(2\varepsilon)] \tag{17}$$

where V_0 is the initial droplet volume and V the droplet volume at the time of interest.

Equation (17) may also be obtained by assuming that transient composition profiles are geometrically similar in the x coordinate according to $(y-y_0)/(y_- - y_0) = \exp[(x^2-1)/(2\varepsilon)]$. For a given volume ratio V_0/V, y_- may be evaluated by employing this relation in the statement of overall mass continuity

$$y_0/3 = \int_0^1 x^2 y\,dx$$

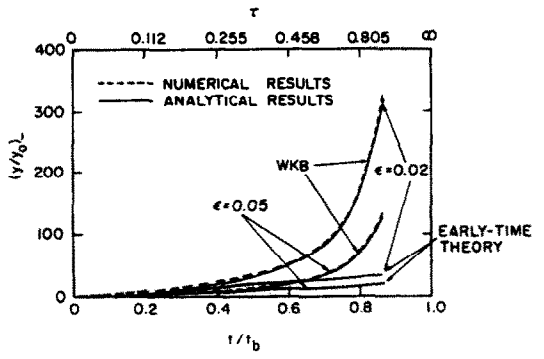

FIG. 5. Comparison of numerical and asymptotic solutions of equation (6) for the surface impurity mass fraction ratio $(y/y_0)_-$ as a function of time.

yielding equation (17) when

$$\int_0^1 x^2 y\,dx$$

is evaluated to leading order in ε.

It is worth noting that at the droplet surface, the boundary-layer analysis predicts that the mass-fraction ratio behaves as $(y/y_0) \approx 1+\varphi+3\varepsilon\varphi^2/2+\ldots$ for $\varphi \to \infty$ (see Appendix B), while equation (15) predicts that $(y/y_0) \approx 1+\tau/\varepsilon+3\tau^2/(2\varepsilon)+\ldots$ for $\tau \to 0$. Since $\varphi = \tau/\varepsilon$, the two expressions agree to this order for the limits $\varphi \to \infty$, $\tau \to 0$.

Shown in Fig. 5 are comparisons of the WKB results from equation (15) with numerical computations and with equation (10) for the surface mass fraction as a function of time. Good agreement between the WKB and numerical results is evident. The improvement over the results shown in Fig. 3 stems from the fact that the effects of volume changes are now taken into account by the WKB method. Figure 6 illustrates comparisons between the numerical results and WKB results for the impurity mass-fraction profiles at the time $t/t_b = 0.6321$ ($\tau = 0.5$) for $\varepsilon = 0.02$ and 0.05. Good agreement between the WKB and numerical results is evident in Fig. 6. Physically,

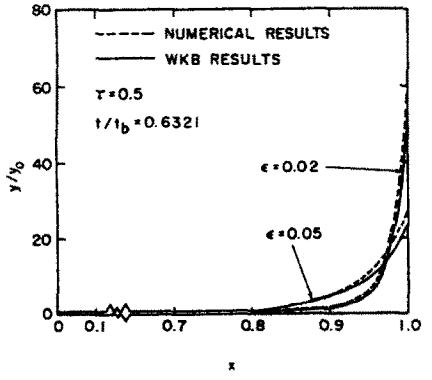

FIG. 6. Comparison of numerical and WKB solutions of equation (6) for the spatial profile of the mass fraction impurity ratio (y/y_0) at the time $t/t_b = 0.6321$.

comparison of equation (9) with equation (15) indicates that, approximately, as the droplet surface regresses, the impurity is swept up by the regressing surface and 'trapped' in a boundary layer with a thickness of $O(\varepsilon)$ (in the transformed space coordinate).

Based on the previous results, it appears reasonable to postulate for the situations considered here that droplet heating is not important during the early portions of the combustion history of an initially quasi-steadily burning droplet, until a critical burn-time ratio $(t/t_b)_c$ is reached when the mass fraction of impurity at the droplet surface approaches unity. As $(t/t_b) \to (t/t_b)_c$, the droplet wants to heat quickly. Because of a finite heat capacity, however, the rate of increase of droplet temperature is limited, and less of the heat input can be used for vaporization, so that the vaporization rate decreases and the flame must contract.

This type of flame contraction has been observed previously [5, 7]. Law and co-workers [5], for example, added a low-volatility surfactant (Span 80) to light liquid hydrocarbon droplets. Droplets burning with Span were observed to burn with d-square-law behavior (following an initial transient) until a critical point was reached at which flame regression suddenly occurred and droplet vaporization slowed considerably. Flame growth was observed after flame contraction, followed by d-square-law behavior until micro-explosion or extinction occurred. The flame growth following flame contraction is attributed to the increased vaporization rates of droplets after completion of droplet heating. The d-square behavior during this period is likely associated with the quasisteady combustion of both Span and the light fuel, as discussed elsewhere [19].

If it is assumed that an impurity mass fraction near unity at the droplet surface is required to produce flame contraction, equation (17) can be used to estimate the reduced droplet volume (V/V_0) at flame contraction for $(1-V/V_0) = O(1)$. For $(1-V/V_0) \ll 1$, equation (10) should be used. For predictive purposes, $y_- = 1$ is employed in equation (17) as a criterion for flame contraction. Equation (17) exhibits reasonable agreement with flame shrinkage data available in the literature [5], as shown in Fig. 7. According to

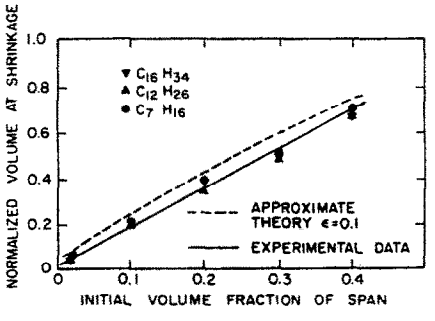

FIG. 7. Comparison of theory (equation (18)) with experimental results [5] for prediction of the normalized droplet volume at flame contraction as a function of the initial impurity volume fraction.

equation (17), the formula for the dashed line in Fig. 7 is simply

$$V/V_0 = y_0/[y_0+3\varepsilon(1-y_0)] \qquad (18)$$

which shows how the critical volume ratio depends on the initial mass fraction y_0 of the low-volatility constituent and on the ratio $(\varepsilon/8)$ of the diffusion coefficient D of the impurity in the liquid to the initial burning-rate constant K_0 of the fuel. The dashed line in Fig. 7 was generated with the assumption that y_0 is equal to the initial volume fraction of Span.

Law and co-workers [5] indicate that for a given value of the initial Span volume fraction, flame contraction occurs at a droplet volume fraction essentially independent of the environmental conditions. The analysis presented here tends to agree with this observation, because $\varepsilon = \varepsilon_0 = 8D/K_0$ depends on K_0, and K_0 should not vary much for droplets vaporizing in a hot environment, until the less volatile component builds to appreciable surface levels, causing significant droplet heating.

6. NON-*d*-SQUARE-LAW COMBUSTION BEHAVIOR

Equations (4)–(6) are non-linearly coupled, making the task of finding simultaneous solutions to these equations formidable. Progress can be made, however, by noting that equation (4) indicates that changes in f will be small when changes in the right-hand side of equation (4), henceforth denoted by G, are small, and that changes of the order of unity in f occur when changes in G are of the order of unity. Increases in y_- increase G, while increases in θ decrease G. The results presented in Section 4 on *d*-square-law combustion assumed that G was constant. Hence, it is instructive to estimate how G varies as combustion proceeds, so that criteria for breakdown of *d*-square-law behavior can be established.

Advantage will be taken of representative magnitudes of parameters to achieve simplification. Thus, analysis can proceed by first noting that for $\theta \ll \alpha_1$, the argument of the exponential appearing in equation (4) can be expanded to yield the approximate relation

$$G = 1+A/[e^f-(1+\nu)] \approx [1+\omega y_-/(1-y_-)]Ee^{-\theta} \qquad (19)$$

where $E = \exp(\alpha_1-\alpha_2)$. Since α_1 typically is of the order of 10, this approximation may be expected to remain valid until θ becomes larger than order unity. Equation (19), when combined with equations (4) and (5), yields

$$\beta\frac{d\theta}{d\tau} \approx (B_0-b_0\theta)/[A/(G-1)+\nu]-1 \qquad (20)$$

subject to $\theta(0) = 0$, where now $B_0 = [c_p(T_\infty-T_0)+qY_{O,\infty}/(\nu_O W_O)]/L_F$ and $b_0 = c_pR_FT_0^2/L_F^2$, since consideration is restricted here to cases in which $\tilde{\varepsilon}_F \approx 1$ and all other $\tilde{\varepsilon}$ are small enough for their contributions to L to be negligible. With attention focused on initially *d*-square combustion, $f_0 = \ln(1+B_0)$, equation (19) requires for $y_0 \ll 1$ that $E \approx 1+A/(B_0-\nu)$. Examination of equation (19) indicates that changes in θ of the order of unity cause changes in f of the order of unity when changes in $\omega y_-/(1-y_-)$ are small compared to unity, while changes in $\omega y_-/(1-y_-)$ of the order of unity cause changes in f of the order of unity if θ is small compared with unity. For θ of the order of unity or less, estimates indicate that $B_0 \gg b_0\theta$ (i.e. B depends weakly upon the droplet temperature) and $A/(G-1) \gg \nu$, allowing equation (20) to be approximated as

$$\beta\frac{d\theta}{d\tau} \approx (1+B_0/A)\{[1+\omega y_-/(1-y_-)]e^{-\theta}-1\}. \qquad (21)$$

Equation (21) can be integrated formally to yield

$$e^\theta \approx 1+\omega e^{-\tau'}\int_0^{\tau'} e^{\tau'}[y_-/(1-y_-)]\,d\tau' \qquad (22)$$

where $\tau' = \tau(1+B_0/A)/\beta$. Equation (22) provides an approximate expression for θ as a function of y_-, provided that y_- is known as a function of τ'. It enables G to be represented approximately as

$$G \approx \frac{[1+\omega y_-/(1-y_-)]E}{1+\omega e^{-\tau'}\int_0^{\tau'} e^{\tau'}[y_-/(1-y_-)]\,d\tau'} \qquad (23)$$

which indicates that G and hence f remain approximately constant when $\omega y_-/(1-y_-) \ll 1$. For $\omega y_-/(1-y_-) \geqslant O(1)$, changes in G are small when the numerator and denominator of the right-hand side of equation (23) change at approximately the same rate, a situation that occurs when $\omega y_-/(1-y_-)$ changes slowly on the τ' time scale. However, if $\omega y_-/(1-y_-)$ changes rapidly on the τ' time scale ($y_- \to 1$ rapidly), then the denominator grows much more slowly than the numerator, and G will change significantly.†

A relevant parameter is thus seen to be $\beta' \equiv \beta/(1+B_0/A)$, the scale factor between the τ and τ' time scales. Since estimates show that in representative situations β' is of the order of 10^{-1} or less, attention will be restricted to small values of β', such that characteristic times for temperature changes are short compared with characteristic times for droplet-size changes.‡ If $\omega y_-/(1-y_-)$ remains small until τ

† It may be remarked in passing that these results can be specialized to pure vaporization without combustion in a hot environment by setting $Y_{O,\infty} = 0$.

‡ In the opposite limit of sufficiently large β' (for example, if the heat capacity of the liquid is large enough), temperature changes develop so slowly that $\theta = 0$ may be employed as a good approximation in equation (19) to convert equation (6) to a temperature-independent problem for addressing the decrease in the burning rate and the consequent flame contraction that occur as y_- approaches unity. To address this problem conveniently by asymptotic methods, ω may reasonably be selected as a small parameter.

becomes of the order of unity (which it can do only if $\varepsilon_0 \gtrsim y_0$, as can be seen by considering equations (10) and (15)), then it is appropriate to use equation (15) in equation (23) to identify conditions under which G will begin to change. When this is done, by asymptotic expansion of the integral in equation (23) by the Laplace method [18] to first order in powers of β' it is then found that G is given approximately by

$$G \approx E/\{1-(\omega\beta')(\mathrm{d}y_-/\mathrm{d}\tau)(1-y_-)^{-1} \times [1-(1-\omega)y_-]^{-1}\} \quad (24)$$

where y_- is evaluated from equation (15). Equation (24) indicates that G increases appreciably, that is, f decreases appreciably, when $1-y_-$ becomes of the order of $\omega\beta'$ ($\mathrm{d}y_-/\mathrm{d}\tau$ is of the order of unity for this case). From equation (15) it then follows that f decreases appreciably when 3τ is within the order of $\omega\beta'$ of $\ln(1+3\varepsilon_0/y_0)$. The time $\tau_c = (1/3)\ln(1+3\varepsilon_0/y_0)$ is a critical time at which y_- approaches unity very closely. Analysis of the resulting decrease in f can proceed by stretching the time variable about τ_c such that changes in τ of the order of $\omega\beta'$ produce changes in the stretched time variable of the order of unity. To this end, the stretched time variable $(\tau-\tau_c)/(\omega\beta')$ may be introduced to analyze equations (6), (19), and (23) simultaneously, with matching to equation (15) imposed as this variable approaches $-\infty$. For $y_0 \ll \varepsilon_0$, this stretching is performed about a large value of τ, such that t is not far from t_b, while for y_0 and ε_0 of the same order, the stretching is about τ and $(t_b-t)/t_b$ of the order of unity.

For $\varepsilon_0 \ll y_0$ it is more appropriate to use equation (9) instead of equation (15) to estimate deviations of f from f_0, since for this case droplet volume changes are not expected to be important before y_- approaches unity. So long as $\varepsilon_0 \ll \beta'\tau' \ll 1$, equation (10) then predicts that $y_- \approx y_0\beta'\tau'/\varepsilon_0$, the substitution of which into equations (19) and (23) yields different results depending on whether $\varepsilon_0/y_0 \ll \beta'$ or $\varepsilon_0/y_0 \gg \beta'$. If $\varepsilon_0/y_0 \ll \beta'$ the approximation

$$A/[\mathrm{e}^f-(1+\nu)]+1 \approx [1+\omega y_0\varphi/(1-y_0\varphi)]E/\{1-[\omega\varepsilon_0/(y_0\beta')][y_0\varphi+\ln(1-y_0\varphi)]\} \quad (25)$$

is obtained. This approximation may be found by noting that for $\varepsilon_0/y_0 \ll \beta'$, $\tau' \ll 1$, allowing the exponentials in equation (23) to be neglected. Conversely, if $\varepsilon_0/y_0 \gg \beta'$ it is found that

$$A/[\mathrm{e}^f-(1+\nu)]+1 \approx E/\{1-(\omega y_0\beta'/\varepsilon_0) \times (1-y_0\varphi)^{-1}[1-(1-\omega)y_0\varphi]^{-1}\}. \quad (26)$$

Equation (26) may be obtained by expanding the integral in equation (23) to first order with the Laplace method, as was done with equation (24). These expressions exhibit appreciable changes in f when $y_0\varphi$ differs from unity by the rather small amount ω for equation (25) or by the smaller amount $\omega y_0\beta'/\varepsilon_0$ for equation (26). Thus, for $\varepsilon_0/y_0 \gg \beta'$ it is appropriate to introduce the stretched time variable $(\varphi-1/y_0)/(\omega\beta'/\varepsilon_0)$ of the order of unity for analyzing the transition, with the solution matched to equation (11) as this variable approaches $-\infty$. On the other hand, for $\varepsilon_0/y_0 \ll \beta'$ the corresponding stretched time is simply $(\varphi-1/y_0)/(\omega/y_0)$, which extends to appreciably earlier times. These predictions are consistent with the results shown in Fig. 2.

At this point in the analysis, some qualitative observations may be made regarding the assumption of spatially uniform droplet temperature profiles. With the assumption of spatially uniform temperatures, order unity decreases in f are predicted to occur when the condition $(1-y_-) \ll 1$ is met. These decreases arise because the droplets require rapid heating as $y_- \to 1$ closely. When non-zero liquid temperature gradients exist, the outer regions of droplets (near $x = 1$) heat faster than the inner regions such that, in effect, less of the liquid mass is heated than if temperature profiles were spatially uniform. Hence, for a given energy flux into a droplet, the droplet surface temperature will increase faster with non-zero liquid temperature gradients than when droplet temperature profiles are spatially uniform. As shown by equation (4), f depends on the variables y_- and θ only; increases in θ lead to increases in f. Thus, it may be argued for the parameter ranges investigated here that the assumption of spatially uniform droplet temperatures provides a slightly conservative estimate for conditions where appreciable decreases in f occur. Allowing for finite-rate liquid heat conduction will allow y_- to approach unity only slightly more closely before f decreases significantly. Since $\mathrm{d}y_-/\mathrm{d}\tau$ is at least of the order of unity for $y_- \to 1$ (see equations (10) and (15)), allowing for finite-rate liquid heat conduction will likely not appreciably change the above estimates for occurrence of decreases in f.

To analytically investigate the occurrence of liquid temperature gradients, it may be argued that the assumption of a uniform droplet temperature is valid as long as characteristic droplet temperature changes occur over long times compared with characteristic thermal diffusion times for the liquid. To evaluate the uniform temperature assumption, especially for the later phase of droplet behavior where the most rapid temperature changes occur, the ratio of a characteristic droplet temperature rise time $t_R = \Delta T/(\mathrm{d}T/\mathrm{d}t)$ to a characteristic thermal diffusion time $t_D = r_l^2 c_{l_l}\rho_l/\lambda$ may be estimated. Here, ΔT is a characteristic droplet temperature change. Droplet temperature profiles may be approximated as spatially uniform when $t_D/t_R \ll 1$. It can be shown that this characteristic time ratio may be expressed as $t_D/t_R = [3/(\Delta\theta)](\partial\theta/\partial x)_-$, where $(\partial\theta/\partial x)_-$ is the non-dimensional temperature gradient on the liquid side of the gas–liquid interface, and $\Delta\theta$ is the characteristic non-dimensional temperature change. The variable $\Delta\theta$ is taken to be of the order of unity, such that liquid-phase temperature gradients may be approximated as spatially uniform when $(\partial\theta/\partial x)_- \ll 1$. By applying energy conservation across the gas–liquid interface, the tem-

perature gradient on the liquid side of the gas–liquid interface may be expressed as

$$\left(\frac{\partial\theta}{\mathrm{d}x}\right)_- = \frac{\lambda_+}{\lambda_-}\frac{c_v}{3c_p}\frac{f}{\beta}\left[\frac{B}{\mathrm{e}^f-1}-1\right] \qquad (27)$$

where λ_+ is the gas thermal conductivity and λ_- the liquid thermal conductivity. With the assumptions used thus far in this analysis, equation (27) may be approximated as

$$\left(\frac{\partial\theta}{\partial x}\right)_- \approx \gamma\left(\frac{G}{E}-1\right)\ln\left(1+\frac{A}{G-1}\right) \qquad (28)$$

where the parameter $\gamma = (\lambda_+/\lambda_-)(1+B_0/A)/b_0$. Equation (28) implies that $(\partial\theta/\partial x)_-$ will be of the order of unity when $(G/E-1)$ is of the order of $1/\gamma$. For the cases considered here, increases in G of the order of unity bring about corresponding decreases in f. Estimates indicate that for typical droplet combustion situations, γ may be of the order of unity, suggesting that liquid temperature gradients may be of the order of unity when changes in f of the order of unity occur. As argued above, non-uniform liquid temperature gradients will likely not significantly influence estimates for when appreciable changes in f occur. For investigation of later combustion behaviors, though, consideration of liquid temperature profiles may be important.

7. VAPORIZATION OF AN INITIALLY PRESENT IMPURITY

The preceding analyses have assumed that vaporization of an initially present impurity was negligible. For the purpose of estimating the amount of impurity in a boundary layer of impurity at the droplet surface it is evident that impurity vaporization is negligible when the mass flow rate of impurity into the boundary layer (from the droplet interior) is much greater than its mass flow rate out of the droplet surface by evaporation. The ratio of the second to the first of these flow rates is simply $\bar{\varepsilon}/y_0$. If the impurity reacts chemically with other species as a fuel in the gas phase according to the single-step chemical reaction given by equation (A1), it is easily shown by algebraic manipulation of equation (A10) that the relation $\bar{\varepsilon} = (1+Y_{\mathrm{F}_+}/Y_{\mathrm{H}_+})$ applies. Here Y_{H_+} is the mass fraction of impurity in the gas phase at the droplet surface. With the assumptions of liquid ideality and applicability of the Clausius–Clapeyron relation with constant vaporization enthalpy for each liquid-phase species, the criterion for neglection of impurity vaporization can be written in terms of dimensional variables as

$$(1/y_- - 1)/(1/y_0 - 1) \gg (P_{\mathrm{bH}}/P) \times \exp\left[(L_{\mathrm{H}}/R_{\mathrm{H}} - L_{\mathrm{F}}/R_{\mathrm{F}})(1/T_{\mathrm{bF}} - 1/T)\right] \qquad (29)$$

where L_{H} is the impurity vaporization enthalpy, R_{H} the impurity gas constant, P_{bH} the vapor pressure of pure impurity at the temperature T_{bF}, and P the ambient pressure. Equation (29) states that impurity vaporization is negligible for y_- and T being sufficiently small, and L_{H} being sufficiently large; as $L_{\mathrm{H}} \to \infty$, P_{bH} decreases sufficiently rapidly such that the right-hand side of equation (29) vanishes.

It was reasoned earlier that sudden flame contraction would be expected if $\omega y_-/(1-y_-)$ approaches unity sufficiently rapidly. Hence, it can be concluded that sudden flame contraction will occur only for a given range of y_0. If y_0 is sufficiently small, then the surface mass fraction of impurity will grow to levels such that equation (29) is violated before the flame-contraction criterion is met (i.e. impurity vaporization becomes sufficiently vigorous to prevent a rapid enough surface buildup of impurity to cause sudden flame contraction). For y_0 sufficiently large, $\omega y_-/(1-y_-)$ is of the order of unity or larger even initially, and sudden flame contraction is not expected to occur.

8. SURFACE CONDENSATION OF GAS-PHASE SPECIES

Migration of high-molecular-weight gas-phase pyrolysis products to the surface of burning hydrocarbon droplets has been suggested as a cause of observed multicomponent-type behavior [11, 12] (i.e. sudden flame contraction followed sometimes by droplet disruption) for initially high-purity single-component fuels. The conjectured situation is one in which gas-phase pyrolysis products miscible with the liquid fuel are absorbed at the droplet surface and diffuse into the droplet interior. The continued deposition of pyrolysis products, as well as the volume change of a burning droplet, will raise the surface mass fraction of these impurities, possibly causing the rapid flame contraction reported in refs. [11, 12] and discussed earlier in this paper. Simplified analyses addressing the possibility of such condensation of gas-phase pyrolysis products on the surface of a burning droplet can be developed in a manner exactly paralleling the preceding analyses.

To proceed with the analysis, it is assumed that all pyrolysis products condensing on the droplet surface can be considered as a single species with a very low volatility relative to the original hydrocarbon fuel. With the previous assumptions used for an initially-present impurity, equation (6) is appropriate in describing the evolution of impurity profiles within a burning droplet, where y is the impurity mass fraction, and $\bar{\varepsilon}$ is negative for impurity deposition onto the droplet surface. All other variables are as previously defined. For further analysis it is assumed that $y_0 = 0$.

To solve equation (6) it is necessary to specify the form of $\bar{\varepsilon}$, which is dependent, for example, on fuel vaporization rates and gas-phase pyrolysis kinetics. Detailed analyses of these processes will not be presented here. Instead, the simplifying assumption that $\bar{\varepsilon}$ is constant will be introduced, allowing equation (6)

to be analyzed by the methods developed in this paper. An objective of such an analysis is to estimate the order-of-magnitude of $\bar{\varepsilon}$ required to produce sudden flame contraction of the type reported in refs. [11, 12].

Earlier it was argued that approximately d-square-law combustion could be expected when the surface mass fraction of impurity was sufficiently small $[\omega y_-/(1-y_-) \ll 1]$. This same criterion will apply here, since the unsteady energy conservation analyses presented in Section 6 remain valid for this situation, so long as $\bar{\varepsilon} \ll 1$ (i.e. impurity returns slowly to the droplet). Hence, for purposes of estimation it can be assumed that droplet vaporization initially follows the d-square-law. Utilization of the transformation $g = -y/\bar{\varepsilon}$, along with the previously-used transformations of the spatial and time coordinates reproduces equation (14) from equation (6). With d-square-law surface regression, approximate solutions to equation (14) can be found using techniques already presented. When $t/t_b \ll 1$, the boundary layer analysis presented in Appendix B is appropriate, yielding for $\varepsilon \ll \tau \ll 1$

$$y \approx \bar{\varepsilon} e^{-\tau} \ln (V/V_0)/(3\varepsilon). \quad (30)$$

When $\tau = O(1)$, the WKB analysis presented in Appendix C is appropriate, yielding

$$y \approx -\bar{\varepsilon}(V_0/V - 1) \exp [(x^2-1)/(2\varepsilon)]/(3\varepsilon). \quad (31)$$

Equations (30) and (31) can be solved to estimate the magnitude of $\bar{\varepsilon}$ required to produce $y_- \sim 1$ at a given volume ratio V_0/V. In refs. [11, 12], flame contraction typically occurs relatively late in the combustion history after a period of approximately d-square-law behavior ($V_0/V \approx 6$, say), implying that equation (31) is appropriate for analyzing these experiments.

Equation (31) states that for y_- and $(V_0/V-1)/3$ of the order of unity, $|\bar{\varepsilon}| = O(\varepsilon)$, requiring that a fraction of $O(\varepsilon)$ of the original liquid fuel condenses on the droplet surface in the form of a miscible low-volatility pyrolysis product. Under typical droplet combustion situations, including those experienced in refs. [11, 12], it is expected that $\varepsilon = 10^{-2}$. Hence, based on this analysis, it appears reasonable to consider the possibility of gas-phase pyrolysis products producing flame contraction behavior of the type observed in refs. [11, 12] as being realistic, since only a small fraction $[O(\varepsilon)]$ of the original droplet mass needs to condense on the droplet surface. More analysis is needed, however, concerning such topics as pyrolysis kinetics, liquid-phase solubilities, and gas-phase transport to determine whether the situation conjectured here actually is realized. For example, gas-phase pyrolysis species diffusivities or net pyrolysis product production rates may be too low to provide pyrolysis-product mass-flux fractions of the magnitudes predicted here to be required for occurrence of sudden flame contraction.

9. SUMMARY AND CONCLUSIONS

This paper has focused on the combustion and evolution of liquid-phase component profiles, vaporization rates, and temperatures of miscible binary droplets containing a high-volatility component ('fuel') and a low-volatility component ('impurity'), with spherical symmetry present in the liquid and gas phases and impurity vaporization neglected. The impurity was treated as being initially present in small amounts, or as returning to the liquid phase from the gas phase at a small rate. In all analyses, droplets were assumed to begin vaporizing with the initial droplet temperature selected such that d-square-law surface regression would occur if there were no buildup of impurity at the droplet surface. In Appendix D, analyses are given regarding the combustion of initially cold droplets, and it is argued that for fuels of sufficiently low molecular weight (e.g. heptane or decane), with sufficiently low initial impurity mass fractions, the effect of droplet surface regression on surface impurity buildup may be neglected during the initial heatup period, so that the results obtained herein continue to apply. Reasoning was presented regarding vaporization of an initially present impurity, and it was shown that impurity vaporization could be neglected when the droplet temperature and the impurity surface mass fraction were sufficiently small. if the impurity was considered to react chemically in the gas phase.

For sufficiently small initial values of the initial impurity mass fraction, numerical integration of the conservation equations for n-decane droplets demonstrated that surface regression would approximately follow the d-square-law until the surface impurity mass fraction closely approached unity, after which the surface regression rate would rapidly decrease and would not follow the d-square-law. For sufficiently large values of the initial impurity mass fraction, the numerical results demonstrated appreciable departures from d-square-law behavior. Asymptotic results for initial and intermediate stages in the droplet vaporization history indicated that when surface regression follows the d-square-law, a boundary layer of impurity grows at the droplet surface. Numerical and asymptotic analyses demonstrated that decreases in the vaporization rates are a result of the surface impurity mass fractions approaching unity. Asymptotic analyses regarding the absorption of a miscible low-volatility component at the surface of a vaporizing droplet suggested that small amounts of material returning to the droplet from the gas phase may be capable of producing the type of flame contraction reported for the combustion of reasonably pure n-decane [11] and impure n-heptane [12] droplets.

The analyses presented demonstrate, for the spherically-symmetric combustion of binary droplets with sufficiently large volatility differentials, that conditions may exist whereby reductions in vaporization rates may be expected, producing flame contraction phenomena similar to those reported in the literature [5, 11, 12], as a consequence of impurity buildup in a liquid boundary layer at the droplet surface. In the

analyses, liquid-phase diffusion was considered to be slow relative to droplet surface regression, and the small parameter $\varepsilon_0 = 8D/K_0$ was identified as being important in characterizing impurity profiles within droplets. Increased surface mass fractions of impurities were shown to lead to droplet heating, and significant reductions in vaporization rates were shown to occur when, because of a finite heat capacity, droplet temperatures could not increase rapidly enough to maintain d-square-law surface regression behavior as the surface mass fraction of impurity approached unity. Asymptotic results predicting the occurrence of flame contraction (equation (18)) exhibit reasonable agreement with data from the literature (Fig. 7). Consideration of vaporization of an initially present combustible impurity indicated that a range of the initial mass fraction of impurity was expected to produce sudden reductions in vaporization rates; with too much impurity initially present, vaporization of the impurity would always be important, and significant droplet heating would not occur, while if too little impurity was present, significant composition changes at the droplet surface would never occur to cause significant droplet heating. Corresponding results apply for an impurity returning to the droplet surface from the gas phase; a small fraction of the original droplet mass ($O(\varepsilon_0)$) needs to return to the droplet in the form of an impurity to reduce vaporization rates.

Further analyses regarding, for example, gas-phase pyrolysis kinetics are needed before definite conclusions may be drawn concerning effects of low-volatility constituents returning from the gas. Further experiments would also be helpful. For example, it could be enlightening to extinguish and capture, for composition analysis, droplets burning in reduced-gravity environments under conditions known to produce flame contraction (e.g. n-decane in atmospheric air [11]), at various times before flame contraction occurs. It would then be possible to evaluate the kinds and amounts of impurities, if any, present in the liquid phase from the gas phase, providing a firmer base from which to draw conclusions.

Further asymptotic analyses would be of interest for describing the phenomena occurring as the surface mass fraction of impurity approaches unity. The relevant time scales have been identified here, but the analyses needed in the stretched time coordinates have not been addressed. There are four cases to be considered, namely $\beta' \gg 1$, $\varepsilon_0/y_0 \ll \beta' \ll 1$, $\beta' \ll \varepsilon_0/y_0 \ll 1$, and $\beta' \ll 1 \lesssim \varepsilon_0/y_0$, the last two of which often will be of greatest physical relevance. The last case includes $\varepsilon_0/y_0 \gg 1$. Pursuit of these analyses is the next step in obtaining complete analytical descriptions of the entire combustion histories of binary fuel droplets of the type considered here.

Acknowledgement—This work was supported by the NASA Microgravity Sciences Program through Contract NAS3-24640 with Princeton University and is part of a joint Princeton–UCSD project on droplet combustion.

REFERENCES

1. G. M. Faeth, Combustion characteristics of blended multicomponent droplets, AIAA Paper A70-18141 (1970).
2. C. K. Law, Multicomponent droplet combustion with rapid internal mixing, *Combust. Flame* **26**, 219–233 (1976).
3. R. B. Landis and A. F. Mills, Effect of internal diffusional resistance on the evaporation of binary droplets, Fifth Int. Heat Transfer Conf., Tokyo, Japan, Paper B7.9 (1974).
4. C. K. Law, Internal boiling and superheating in vaporizing multicomponent droplets, *A.I.Ch.E. Jl* **24**, 626–632 (1978).
5. C. H. Wang, X. Q. Liu and C. K. Law, Combustion and microexplosion of freely falling multicomponent droplets, *Combust. Flame* **56**, 175–197 (1984).
6. A. L. Randolph, A. Makino and C. K. Law, Liquid-phase diffusional resistance in multicomponent droplet gasification, Twenty-first Symp. (Int.) on Combustion, The Combustion Institute, Pittsburgh, pp. 601–608 (1986).
7. T. Niioka and J. Sato, Combustion and microexplosion behavior of miscible fuel droplets under high pressure, Twenty-first Symp. (Int.) on Combustion, The Combustion Institute, Pittsburgh, pp. 625–631 (1986).
8. J. C. Lasheras, A. C. Fernandez-Pello and F. L. Dryer, Experimental observations on the disruptive combustion of free droplets of multicomponent fuels, *Combust. Sci. Technol.* **22**, 195–209 (1980).
9. L. T. Yap, I. M. Kennedy and F. L. Dryer, Disruptive and micro-explosive combustion of free droplets in highly convective environments, *Combust. Sci. Technol.* **41**, 291–313 (1984).
10. J. C. Yang and C. T. Avedisian, The combustion of unsupported heptane/hexadecane mixture droplets at low gravity, Sibley School of Mechanical and Aerospace Engineering Report E-88-02, Cornell University (January 1988).
11. B. D. Shaw, F. L. Dryer, F. A. Williams and J. B. Haggard, Jr., Sooting and disruption in spherically symmetrical combustion of decane droplets in air, *Acta Astronautica* **17**, 1195–1202 (1988).
12. J. B. Haggard, Jr., Personal communication (1988).
13. W. A. Sirignano and C. K. Law, Transient heating and liquid-phase mass diffusion in fuel droplet vaporization. In *Advances in Chemistry Series*, No. 166 (Edited by J. T. Zung). American Chemistry Society, Washington, DC (1978).
14. F. A. Williams, *Combustion Theory* (2nd Edn), Chap. 1 and Appendices A and E. Benjamin Cummings, Menlo Park, California (1985).
15. B. Carnahan, H. A. Luther and J. O. Wilkes, *Applied Numerical Methods*, Chaps 6 and 7. Wiley, New York (1969).
16. A. Makino and C. K. Law, On the controlling parameter in the gasification behavior of multicomponent droplets, *Combust. Flame* **73**, 331–336 (1988).
17. IMSL User's Manual, Math/Library, Version 1.0 (April 1987).
18. C. M. Bender and S. A. Orszag, *Advanced Mathematical Methods for Scientists and Engineers*, Chaps 6 and 10. McGraw-Hill, New York (1978).
19. C. K. Law and H. K. Law, A d^2-law for multicomponent droplet vaporization and combustion, *AIAA J.* **20**, 522–527 (1981).
20. H. S. Carslaw and J. C. Jaeger, *Conduction of Heat in Solids* (2nd Edn), Appendix V. Oxford University Press, London (1959).
21. B. D. Shaw, Ph.D. Dissertation, Mechanical and Aerospace Engineering Department, Princeton University, Princeton, New Jersey (1989).

APPENDIX A. DROPLET VAPORIZATION WITH A QUASISTEADY GAS PHASE

With the simplifications that the gas-phase Lewis number is unity, body forces are negligible, radiant heat flux is negligible, that the specific heat and binary diffusion coefficients of all species are constant and equal, that diffusion is described by Fick's law [14], and that gas-phase chemical changes occur by a single-step mechanism

$$\sum_{i=1}^{N} \nu_i' S_i \rightarrow \sum_{i=1}^{N} \nu_i'' S_i \tag{A1}$$

(S_i = species i) solutions to the quasisteady gas-phase conservation equations can be conveniently described in terms of 'coupling functions' [14] defined by

$$\Omega = \alpha_i - \alpha_j \tag{A2}$$

where

$$\alpha_i = Y_i/[W_i(\nu_i'' - \nu_i')] \tag{A3a}$$

for species conservation, or where

$$\alpha_j = c_p(T - T_+)/q \tag{A3b}$$

for energy conservation. Here, Y_i is the mass fraction of species i, W_i the molecular weight of species i, T_+ the temperature of the droplet surface, c_p the specific heat at constant pressure, and q the standard heat of reaction for the fuel ($q = \Sigma_{i=1}^{N} h_i^0 W_i(\nu_i' - \nu_i'')$, where h_i^0 is the enthalpy of formation of the ith species). In terms of the dimensionless radial coordinate

$$f = \int_r^{\infty} [\dot{m}c_p/(4\pi r^2\lambda)]\,dr \approx \dot{m}c_p/(4\pi r\lambda) \tag{A4}$$

where r is the physical radial coordinate, $\dot{m}$ the droplet vaporization rate, and λ the gas-phase thermal conductivity, the solution for β in spherical coordinates yields the relation

$$e^{f_+} - 1 = (\Omega_+ - \Omega_\infty)/(\partial\Omega/\partial f)_+ \tag{A5}$$

where the subscripts ∞ and $+$ indicate values in the ambient environment and at the droplet surface ($r = r_1$), respectively.

With the assumption that oxidizer is present at the droplet surface in negligible amounts, the gas-phase temperature gradient at the droplet surface can be evaluated by using the coupling function

$$\Omega = c_p(T - T_+)/q + Y_O/(\nu_O W_O) \tag{A6}$$

(where the subscript O denotes oxidizer) in equation (A5), yielding

$$(r\partial T/\partial r)_+ = f_+[(T_\infty - T_+) + qY_{O,\infty}/(\nu_O W_O c_p)]/[e^{f_+} - 1]. \tag{A7}$$

The subscript $+$ on f is omitted for brevity when this formula is employed in the main text. With the definition $\bar{L} = L - c_r r_1(dT_+/dt)/[3(dr_1/dt)]$, equation (1) allows equation (A7) to be rewritten as

$$e^{f_+} - 1 = [c_p(T_\infty - T_+) + Y_{O,\infty}q/(\nu_O W_O)]/\bar{L} \tag{A8}$$

where $\bar{L}$ is the effective enthalpy of vaporization of the liquid. By using the coupling function

$$\Omega = Y_{F_i}/(\nu_{F_i} W_{F_i}) - Y_O/(\nu_O W_O) \tag{A9}$$

(the subscript F_i denotes the ith fuel component) in equation (A5), it can be shown that the relation

$$e^{f_+} - 1 = [Y_{F_{i+}} + Y_{O,\infty}\nu_{F_i}W_{F_i}/(\nu_O W_O)]/[\tilde{\varepsilon}_{F_i} - Y_{F_+}] \tag{A10}$$

is valid when it can be assumed that oxidizer and fuel are present in negligible amounts at the droplet surface and in the ambient atmosphere, respectively, and where $\tilde{\varepsilon}_{F_i}$ is the mass-flux fraction of the ith fuel component at the droplet surface. For gas-phase products that do not enter the liquid phase, consideration of the coupling function

$$\Omega = Y_O/(\nu_O W_O) + Y_{P_i}/(\nu_{P_i} W_{P_i}) \tag{A11}$$

allows the relation

$$Y_{P_{i+}} = \nu_{P_i} W_{P_i} Y_{O,\infty}\, e^{-f_+}/(\nu_O W_O) \tag{A12}$$

to be found from equation (A5) (with the assumption that product concentrations are negligible in the atmosphere). The subscript P_i indicates the product i. The mass fraction at the droplet surface of an inert gas present in the environment can be evaluated with the relation

$$Y_{I_+} = 1 - \sum Y_{F_{i+}} - \sum Y_{P_{j+}} = e^{-f_+}(1 - Y_{O,\infty}) \tag{A13}$$

where the subscript I denotes the inert species.

For the analysis presented in this paper, it has been assumed that the liquid is ideal and that the Clausius–Clapeyron relation with a constant vaporization enthalpy is valid, yielding the phase-equilibrium relation

$$X_{F_{i+}} = X_{F_{i-}} \exp[L_{i+}(1/T_{b_{i+}} - 1/T_+)R_{F_i}] \tag{A14}$$

where X is the mole fraction, T_b the boiling temperature at the ambient pressure, and R the gas constant. Equations (A8), (A10), and (A12)–(A14), coupled with the identity

$$X_i = (Y_i/W_i)\Big/\sum_j (Y_j/W_j) \tag{A15}$$

were used to generate the results presented in the main text.

A transfer number $\bar{B}$ may be defined as

$$\bar{B} = e^{f_+} - 1 \tag{A16}$$

whence the burning-rate constant K, defined by

$$K = -8r_1(dr_1/dt) \tag{A17}$$

is readily found by using relations (A4) and (A16) to give

$$K = [8\lambda/(\rho_l c_p)]\ln(1 + \bar{B}). \tag{A18}$$

Here λ/c_p has been assumed constant, and ρ_l is the liquid density. When $\bar{B}$ is independent of time, K is constant, yielding the familiar d-square-law

$$d^2 = d_0^2 - Kt. \tag{A19}$$

Here, d is the droplet diameter at time t, and d_0 the droplet diameter at $t = 0$.

APPENDIX B. EARLY-TIME BOUNDARY-LAYER ANALYSIS

To analyze equation (6) approximately for $\tau \rightarrow 0$, $\varepsilon \rightarrow 0$, it is convenient to transform the dependent variable using $h = y/y_0 - 1$, yielding the problem

$$\frac{\partial h}{\partial \tau} = \varepsilon\frac{\partial^2 h}{\partial x^2} + \left[\frac{2\varepsilon}{x} - x\right]\frac{\partial h}{\partial x}, \quad \left[\varepsilon\frac{\partial h}{\partial x} - h\right]_{x=1} = 1,$$

$$\left[\frac{\partial h}{\partial x}\right]_{x=0} = 0, \quad h(x,0) = 0. \tag{B1}$$

To analyze this problem, an 'outer expansion' of the form

$$h = H_0 + \varepsilon H_1 + \ldots \tag{B2}$$

can be assumed. Substitution of equation (B2) into equation (B1) and equating terms of equal order of ε yields a series of outer problems, namely, for $n = 0$

$$\frac{\partial H_0}{\partial \tau} + x\frac{\partial H_0}{\partial x} = 0, \quad \left[\frac{\partial H_0}{\partial x}\right]_{x=0} = 0, \quad H_0(x,0) = 0 \tag{B3}$$

and for $n = 1, 2, \ldots$

$$\frac{\partial H_n}{\partial \tau} + x\frac{\partial H_n}{\partial x} = \frac{\partial^2 H_{n-1}}{\partial x^2} + \frac{2}{x}\frac{\partial H_{n-1}}{\partial x}, \quad \left[\frac{\partial H_n}{\partial x}\right]_{x=0} = 0,$$

$$H_n(x,0) = 0. \tag{B4}$$

Because of the expected boundary layer at $x = 1$, the boundary condition at $x = 1$ has been neglected. The general solution to the leading-order outer problem is

$$H_0 = H_0[\tau - \ln(x)]. \tag{B5}$$

To satisfy the boundary and initial conditions for the leading-order problem, the condition $H_0 = 0$ must be enforced. It is found from equations (B3) and (B4) that $H_n = 0$ for all n for the outer problem. This analysis has treated τ of the order of unity, instead of φ (defined below) of the order of unity. If instead φ is taken of the order of unity the same result is obtained even more simply.

The analysis in the boundary layer can be carried out with the 'stretching' transformation $x = 1 - \delta z$ ($\delta = \delta(\varepsilon) \ll 1$) and by assuming that the inner expansion

$$h = h_0 + \varepsilon h_1 + \ldots \tag{B6}$$

is valid. Substitution of equation (B6) into equation (B1) and equating terms of equal order of ε yields for the first two inner problems

$$\frac{\partial h_0}{\partial \varphi} = \frac{\partial^2 h_0}{\partial z^2} + \frac{\partial h_0}{\partial z}, \quad \left[\frac{\partial h_0}{\partial z} + h_0\right]_{z=0} = -1, \quad h_0(z,0) = 0,$$
$$h_0(z \to \infty) = 0 \tag{B7}$$

and

$$\frac{\partial h_1}{\partial \varphi} - \frac{\partial^2 h_1}{\partial z^2} - \frac{\partial h_1}{\partial z} = -(z+2)\frac{\partial h_0}{\partial z}, \quad \left[\frac{\partial h_1}{\partial z} + h_1\right]_{z=0} = 0,$$
$$h_1(z,0) = 0, \quad h_1(z \to \infty) = 0 \tag{B8}$$

where $\varphi = \tau/\varepsilon$ and $\delta = \varepsilon$ for a distinguished limit. Solution of the leading-order problem is accomplished by taking a Laplace transform in the time coordinate to yield the problem

$$\frac{d^2\bar{h}_0}{dz^2} + \frac{d\bar{h}_0}{dz} - s\bar{h}_0 = 0, \quad \left[\frac{d\bar{h}_0}{dz} + \bar{h}_0\right]_{z=0} = -1/s,$$
$$\bar{h}_0(z \to \infty) = 0 \tag{B9}$$

where s and $\bar{h}_0$ are defined by the Laplace transform

$$\bar{h}_0(s,z) = \int_0^\infty e^{-s\varphi} h_0(\varphi, z)\, d\varphi. \tag{B10}$$

The solution to equation (B9) is

$$\bar{h}_0(s,z) = \exp[-(\sqrt{(s+1/4)} + 1/2)z]/[s(\sqrt{(s+1/4)} - 1/2)]. \tag{B11}$$

An explicit inversion for equation (B11) was not found in the tables of Laplace transforms. However, inversion of equation (B11) can be accomplished by noting that the function

$$\exp[-(\sqrt{(s+1/4)} + 1/2)z]/[s(\sqrt{(s+1/4)} + b)] \tag{B12}$$

has the inverse Laplace transform [20]

$$\operatorname{erfc}[z/\sqrt{(4\varphi)} + \sqrt{(\varphi/4)}]/(2b-1) + \{(b/2 - 1/4)\, e^{-z}$$
$$\times \operatorname{erfc}[z/\sqrt{(4\varphi)} - \sqrt{(\varphi/4)}] - (b)\exp[z(b-1/2) + \varphi(b^2 - 1/4)]$$
$$\times \operatorname{erfc}[z/\sqrt{(4\varphi)} + b\sqrt{\varphi}]\}/(b^2 - 1/4) \tag{B13}$$

for $b^2 \neq 1/4$. The inverse transform of equation (B11) can be found by evaluating equation (B13) for the limit $b \to -1/2$, yielding the leading-order solution

$$h_0 = e^{-z}(\varphi - z + 1)\{1 - \operatorname{erfc}[\sqrt{(\varphi/4)} - z/\sqrt{(4\varphi)}]/2\}$$
$$- \operatorname{erfc}[z/\sqrt{(4\varphi)} + \sqrt{(\varphi/4)}]/2 + \sqrt{(\varphi/\pi)}$$
$$\times \exp[-(z^2/\varphi + 2z + \varphi)/4] \tag{B14}$$

a result verifiable by contour integration in the complex s-plane [21] or by substitution back into equation (B7).

The next term (h_1) in the inner expansion can be evaluated by taking the Laplace transform of equation (B8) to yield the problem

$$\frac{d^2\bar{h}_1}{dz^2} + \frac{d\bar{h}_1}{dz} - s\bar{h}_1 = -(z+2)[\sqrt{(s+1/4)} + 1/2]$$
$$\times \exp[-(\sqrt{(s+1/4)} + 1/2)z]/[s(\sqrt{(s+1/4)} - 1/2)]$$
$$\left[\frac{d\bar{h}_1}{dz} + \bar{h}_1\right]_{z=0} = 0, \quad \bar{h}_1(z \to \infty) = 0 \tag{B15}$$

where $\bar{h}_1$ is the Laplace transform of h_1. At the droplet surface ($z = 0$) the solution to equation (B15) is

$$\bar{h}_1 = (\sqrt{(s+1/4)} + 1/2)(4\sqrt{(s+1/4)} + 1)/$$
$$[4s(s+1/4)(\sqrt{(s+1/4)} - 1/2)^2]. \tag{B16}$$

Taylor expansion of the term $[\sqrt{(s+1/4)} - 1/2]$ in equation (B16) illustrates that $s = 0$ is a third-order pole, showing that $h_1 \sim \varphi^2$ for $\varphi \to \infty$. The leading-order behavior of equation (B16) for $s \to 0$ is $\bar{h}_1 \approx 3/s^3$, indicating that $h_1 \approx 3\varphi^2/2$ for $\varphi \to \infty$.

APPENDIX C. WKB ANALYSIS

Laplace transformation in the time coordinate τ of equation (14) yields the problem

$$\varepsilon\frac{d^2\bar{g}}{dx^2} + \left(\frac{2\varepsilon}{x} - x\right)\frac{d\bar{g}}{dx} - s\bar{g} = 0, \quad \left[\varepsilon\frac{d\bar{g}}{dx} - \bar{g}\right]_{x=1} = 1/s,$$
$$\left[\frac{d\bar{g}}{dx}\right]_{x=0} = 0 \tag{C1}$$

where $\bar{g}$ is the Laplace transform of g. An exact solution to equation (C1) can be found (by a Frobenius series expansion, say, or by transformation to the parabolic cylinder equation), but the complexity of the solution discourages the inverse Laplace transformation from being performed. An approximate solution to equation (C1) can be found, however, by using WKB analysis [18] for the limit $\varepsilon \to 0$, which is amenable to inverse Laplace transformation.

To analyze equation (C1) approximately for $\varepsilon \to 0$, the WKB-type representation

$$\bar{g} = \exp\left(\sum_{n=0}^{\infty} \delta^{n-1} S_n\right) \tag{C2}$$

can be inserted into equation (C1), yielding

$$(\varepsilon/\delta)[S_0'^2 + \delta S_1'^2 + \ldots] + (\varepsilon/\delta^2)[(S_0')^2 + 2\delta S_1' S_0' + \ldots]$$
$$+ [2\varepsilon/(\delta x)][S_0' + \delta S_1' + \ldots] - (x/\delta)[S_0' + \delta S_1' + \ldots] - s = 0 \tag{C3}$$

where $\delta \ll 1$, and primes denote differentiation with respect to x. The transform variable s is taken to be of the order of unity, corresponding to intermediate values of τ. A distinguished limit for equation (C3) is found with $\delta = \varepsilon$, yielding the leading-order problem

$$(S_0')^2 - xS_0' = 0 \tag{C4}$$

which has the solutions $S_0 = C_1$, $S_0 = x^2/2$, where C_1 is a constant. The first-order problem from equation (C3) is found to be

$$S_0'' + 2S_0'S_1' + (2/x)S_0' - xS_1' - s = 0. \tag{C5}$$

For $S_0 = C_1$ the solution to equation (C5) is $S_1 = \ln(x^{-s})$, while for $S_0 = x^2/2$ the solution to equation (C5) is $S_1 = \ln(x^{s-3})$. The physical-optics approximation for the solution to equation (C1) can then be written as

$$\bar{g} \approx a_1 x^{-s} + a_2 x^{s-3} e^{x^2/(2\varepsilon)} \tag{C6}$$

where a_1 and a_2 are constants. For equation (C6) to remain bounded as $x \to 0$ for the real part Re (s) being positive, the conditions $a_1 = 0$ and Re (s) > 3 must be imposed. Sub-

stitution of equation (C6) (with $a_1 = 0$) into the first boundary condition in equation (C1) allows the constant a_2 to be evaluated, yielding the physical-optics approximation

$$\bar{g} \approx x^{s-3}\{\exp[(x^2-1)/(2\varepsilon)]\}/[\varepsilon s(s-3)]. \quad \text{(C7)}$$

The inverse Laplace transform of equation (C7) is

$$g \approx [1/(3\varepsilon)](e^{3\tau} - 1/x^3)\exp[(x^2-1)/(2\varepsilon)]H[\tau + \ln(x)] \quad \text{(C8)}$$

where $H[\tau+\ln(x)]$ is the Heaviside step function, namely $H[\tau+\ln(x)] = 1$ for $e^{\tau} > 1/x$, while $H[\tau+\ln(x)] = 0$ for $e^{\tau} < 1/x$. Equation (C8) implies that the leading edge of an impurity diffusion wave reaches the location x within the droplet at the non-dimensional time $\tau = \ln(1/x)$, with the bulk of the impurity being 'swept up' into a boundary layer with thickness of order ε (in the x coordinate) as the droplet surface regresses. Hence, for $\tau \gg \varepsilon$, equation (C8) can be adequately represented by the function

$$g \approx [1/(3\varepsilon)](e^{3\tau} - 1)\exp[(x^2-1)/(2\varepsilon)] \quad \text{(C9)}$$

for $\varepsilon \to 0$, since g becomes exponentially small for $(1-x) > O(\varepsilon)$.

For $\tau \gg 1$ the solution in equation (C9) becomes approximately

$$g \approx [e^{3\tau}/(3\varepsilon)]\exp[(x^2-1)/(2\varepsilon)]. \quad \text{(C10)}$$

Equation (C10) in fact satisfies the differential equation and the boundary condition at $x = 0$ in equation (14) exactly, failing only to satisfy the initial condition and the boundary condition at the droplet surface. At the droplet surface, equation (C10) gives $[\varepsilon(dg/dx) - g]_- = 0$. Since $g_- \gg 1$ for $\tau \gg 1$, the relation $[\varepsilon(dg/dx) - g]_- = 0$ may be taken to represent an asymptotic large-time limit for the surface boundary condition in equation (14). Hence, for large τ the solution may be expected to be proportional to that given in equation (C10), irrespective of the initial condition, with the constant of proportionality determined by the total amount of impurity swept up by the droplet as its diameter becomes small compared with the initial diameter, that is, by the total amount of impurity present in the droplet.

APPENDIX D. COMBUSTION OF INITIALLY COLD DROPLETS

The results presented assumed that the initial temperature of a droplet was sufficiently high that d-square-law combustion would occur if there were no buildup of impurity at the droplet surface. This restriction could be construed to preclude these results from being applicable to situations in which droplets are initially cold, such that substantial droplet heating must occur before vigorous vaporization begins. Results in the literature [13] suggest that for pure single-component hydrocarbon droplets of sufficiently low molecular weight, combustion (or vaporization in a hot environment) can essentially be divided into two periods. The first period is characterized by low vaporization rates with rapid droplet heating, while the second period is characterized by vigorous vaporization with slow heating, with the transition between the two periods occurring rapidly. In the first period, since vaporization rates are low, the droplet surface does not regress appreciably. There is no reason to suspect that small amounts of impurity would alter these results.

Therefore, consider the solution to equation (21) subject to $\theta(0) = \theta_0 \neq 0$ for the case in which no impurity is present; namely

$$(r_{l0}/r_l) \approx [(e^{\theta_0} - 1)/(e^{\theta} - 1)]^{\beta'}. \quad \text{(D1)}$$

Equation (D1), when coupled with equation (19), yields an approximate relation for f, namely

$$A/[e^f - (1+\nu)] \approx (1 + A/B_0)/[1 + (e^{\theta_0} - 1)(r_l/r_{l0})^{1/\beta'}] - 1. \quad \text{(D2)}$$

For $\beta' \ll 1$ and $|e^{\theta_0} - 1| = O(1)$, the denominator on the right-hand side of equation (D2) rapidly approaches unity with small decreases in r_l/r_{l0}, supporting the assumption of a stationary droplet surface as initial droplet heating progresses. When $\beta' = O(1)$, equation (D2) predicts that f will vary significantly from droplet-heating effects over a large portion of the droplet lifetime until $|(r_l/r_{l0})^{1/\beta'}[e^{\theta_0} - 1]| \ll 1$. For $\beta' \gg 1$ and $|e^{\theta_0} - 1| = O(1)$ equation (D2) predicts that droplet heating is slow so that d-square-law behavior will be followed for most of the droplet lifetime, until the end, when significant heating will occur. Estimates indicate that $\beta' \ll 1$ for typical droplet combustion situations at 1 atm. Increases in β' may occur, for example, as a result of using heavier fuels, lowering the oxidizer concentration in the environment, or increasing the pressure.

THEORIE DE L'INFLUENCE D'UNE IMPURETE SOLUBLE A FAIBLE VOLATILITE SUR LA COMBUSTION, A SYMETRIE SPHERIQUE, DE GOUTTELETTES COMBUSTIBLES

Résumé—On analyse l'évolution de la température et des profils de fraction en masse de la phase liquide pendant la combustion des gouttelettes combustibles composées de mélanges miscibles binaires de constituants à faible et à forte volatilité, avec de petites fractions initiales de matériau à faible volatilité, ou avec introduction lente de matériau à faible volatilité dans la phase liquide par absorption de la phase gazeuse. La phase gazeuse est supposée être permanente et la température du liquide spatialement uniforme. On traite comme un paramètre petit le rapport du coefficient de diffusion de la phase liquide à la constante initiale de la vitesse de combustion. On développe les analyses asymptotiques vis-à-vis de ce paramètre, et les équations de conservation sont intégrées numériquement en obtenant des descriptions de l'histoire de la combustion. On montre qu'à la surface de la goutte se forme une couche limite dans laquelle la fraction de masse du composant à faible volatilité augmente avec le temps. Les résultats sont utilisés pour expliquer qualitativement des observations de contraction de flamme et de rupture de liquide dans la combustion de la gouttelette.

THEORIE FÜR DEN EINFLUSS EINER LEICHTFLÜCHTIGEN LÖSLICHEN BEIMENGUNG AUF DIE KUGELFÖRMIG-SYMMETRISCHE VERBRENNUNG VON BRENNSTOFF-TRÖPFCHEN

Zusammenfassung—Es wird die Entwicklung von Konzentrationsprofil und Temperatur in der flüssigen Phase während der Verbrennung von Brennstoff-Tröpfchen berechnet. Der Brennstoff besteht aus binären mischbaren Vermengungen von leichtflüchtigen und schwerflüchtigen Komponenten, wobei entweder das anfängliche Massen-Verhältnis des leichtflüchtigen Materials gering ist oder das leichter flüchtige Material durch Absorption aus der Gasphase in die flüssige Phase gelangt. Die Gasphase wird als quasi-ruhend angenommen, die Temperatur der Flüssigkeit als räumlich konstant. Das Verhältnis von Diffusionskoeffizient der flüssigen Phase zur anfänglichen Verbrennungsgeschwindigkeits-Konstanten wird als klein betrachtet. Dieser Parameter wird asymptotisch entwickelt. Der zeitliche Ablauf der Verbrennung ergibt sich durch eine numerische Integration der Erhaltungsgleichungen. Es wird gezeigt, daß an der Oberfläche des Tröpfchens eine Grenzschicht entsteht, in der das Massenverhältnis der leichter flüchtigen Komponente mit der Zeit zunimmt. Mit Hilfe der Ergebnisse werden einige Beobachtungen zum Einschnüren von Flammen und zum Zerteilen von Flüssigkeiten bei der Verbrennung von Tröpfchen qualitativ erklärt.

ТЕОРИЯ ВЛИЯНИЯ РАСТВОРИМОЙ ПРИМЕСИ С НИЗКОЙ ЛЕТУЧЕСТЬЮ НА СФЕРИЧЕСКИ-СИММЕТРИЧНОЕ СГОРАНИЕ КАПЕЛЬ ТОПЛИВА

Аннотация—Анализируется эволюция профилей массовой доли жидкой фазы и температуры в процессе сгорания капель топлива, состоящего из бинарных растворимых смесей компонентов с низкой и высокой летучестью, при малых начальных массовых долях низколетучего материала или медленном введении этого материала в жидкую фазу посредством абсорбции из газовой фазы. Предполагается, что газовая фаза является квазистационарной, а температура жидкости—пространственно однородной. Отношение коэффициента диффузии жидкости к константе скорости сгорания считается малым параметром. Для описания характера процесса сгорания разрабатывается метод асимптотического анализа на основе данного параметра и численно интегрируются уравнения сохранения. Показано, что у поверхности капли возникает пограничный слой с увеличивающейся во времени массовой долей низколетучего компонента. Полученные результаты используются для качественного объяснения некоторых условий сжатия пламени и разрыва жидкости, наблюдаемых в процессе капельного сгорания.